

Water Resources Research®

RESEARCH ARTICLE

10.1029/2024WR038560

Cycles in Hydrologic Intensification and De-Intensification Create Instabilities in Spring Nitrate-N Export C-Q Relationships in Northern Temperate Forests



Key Points:

- Cycling between hydrologic intensification and de-intensification destabilizes spring nitrate-N export and C-Q relationships in northern temperate forests
- C-Q relationships were stable (C and Q declining in sync) during intensification but shifted to instability during de-intensification as Q increased and N sources shifted from proximal, organized sources to distal, disorganized sources
- Wetlands help stabilize fluctuations in nitrate-N export, ensuring consistent C-Q dynamics despite hydrologic intensification-de-intensification cycles

I. F. Creed¹ , D. A. Aldred¹ , J. A. Leach² , K. L. Webster², and M. Bierozza³ 

¹Department of Physical and Environmental Sciences, University of Toronto Scarborough, Toronto, ON, Canada, ²Natural Resources Canada, Canadian Forest Service, Great Lakes Forestry Centre, Sault Ste. Marie, ON, Canada, ³Swedish University of Agricultural Sciences, Uppsala, Sweden

Supporting Information:

Supporting Information may be found in the online version of this article.

Correspondence to:

I. F. Creed,
irena.creed@utoronto.ca

Citation:

Creed, I. F., Aldred, D. A., Leach, J. A., Webster, K. L., & Bierozza, M. (2025). Cycles in hydrologic intensification and de-intensification create instabilities in spring nitrate-N export C-Q relationships in northern temperate forests. *Water Resources Research*, 61, e2024WR038560. <https://doi.org/10.1029/2024WR038560>

Received 30 JUL 2024

Accepted 30 JAN 2025

Author Contributions:

Conceptualization: I. F. Creed
Data curation: D. A. Aldred
Formal analysis: D. A. Aldred
Funding acquisition: I. F. Creed
Investigation: D. A. Aldred
Methodology: I. F. Creed, D. A. Aldred, M. Bierozza
Project administration: I. F. Creed

© 2025. The Author(s).

This is an open access article under the terms of the [Creative Commons Attribution-NonCommercial-NoDerivs License](https://creativecommons.org/licenses/by/4.0/), which permits use and distribution in any medium, provided the original work is properly cited, the use is non-commercial and no modifications or adaptations are made.

Abstract Northern temperate forests are experiencing changes from climate and acidification recovery that influence catchment nitrate-nitrogen (N) flushing behavior. N flushing behavior is characterized by metrics such as: (a) N flushing time—the exponential decrease in stream N concentration during the peak snowmelt episode; and (b) N concentration (C) and discharge (Q) hysteresis metrics—flushing index (FI) and hysteresis index (HI)—representing the slope, direction, and amplitude of the C-Q loop. We hypothesized that climate-driven hydrologic intensification results in longer N flushing times, lower FI (less flushing to more diluting), and lower HI (less proximal to more distal N sources). We tested this hypothesis using four decades of data from two headwater catchments. Hydrologic intensification was estimated by changes in the ratio of potential evapotranspiration to precipitation and the ratio of actual evapotranspiration to precipitation. From 1982 to 2005, a period characterized by hydrologic intensification and a decline in atmospheric acidic deposition, we observed a decrease in C and Q. This led to stable C-Q patterns that reflected the flushing (positive FI) of proximal N sources (positive HI). However, from 2006 to 2019, a period of hydrologic de-intensification coupled with an ongoing decline in atmospheric acidic deposition was associated with a continued decrease in C but an increase in Q, leading to unstable C-Q patterns that reflected a shift from proximal (positive HI) toward distal N sources (negative HI). C-Q instability was less variable in the catchment with a large wetland, indicating the potential of wetlands to buffer against changing climate conditions.

1. Introduction

Climate change impacts catchment hydrologic episodes, with implications for downstream surface waters. Hydrologic episodes are pulses of water that promote hydrologically driven terrestrial export of biogeochemical constituents to surface waters (Cirmo & McDonnell, 1997). In northern temperate forests, major hydrologic episodes occur during the vernal window, a period that marks the end of winter and the start of the growing season, characterized by rapid transitions in ecosystem energy, water, nutrient, and carbon dynamics (Contosta et al., 2017). Conversely, the autumnal window signifies the end of the growing season and the onset of winter, also involving quick transitions in ecosystem dynamics (Creed, Hwang, et al., 2015; Creed, McKnight, et al., 2015). The shift from stationary (oscillations) to non-stationary (trends) in climatic conditions (Milly et al., 2008) may change the patterns of hydrologic episodes and amplify alterations in hydrologically driven terrestrial export of biogeochemical constituents (Li et al., 2024; van Vliet et al., 2023). These patterns are already being affected by acidification and subsequent recovery in these forests (Gilliam et al., 2019).

Creed et al. (1996) proposed the nitrate-nitrogen (N) flushing hypothesis to clarify N export behavior from headwater catchments in a northern temperate forest. According to the N flushing hypothesis, an N-enriched upper soil layer forms after a period of low N demand by the forest, with some N draining as groundwater translocates N from the upper soil layer into deeper hydrologic flow pathways, which are released slowly over the year. During a hydrologic episode, such as spring snowmelt or autumn stormflow, this N-enriched upper layer is flushed by a combination of saturated subsurface and surface flow, resulting in a significant export of N to surface waters (Creed et al., 1996). N flushing is captured in the characteristic time constant, the time interval required for a decline in peak N concentration in discharge water to 37% (e^{-1}) of its initial concentration (Boyer et al., 1998). A comparison of the characteristic time constant among different catchments revealed that catchment topography and its influence on variable source area dynamics (representing the intersection of saturated throughflow with N near or at the soil surface (Creed & Band, 1998b) determined the potential for hydrologic expansion into new

Resources: I. F. Creed, J. A. Leach, K. L. Webster
Supervision: I. F. Creed
Visualization: D. A. Aldred
Writing – original draft: I. F. Creed, D. A. Aldred, M. Bierzoza
Writing – review & editing: I. F. Creed, D. A. Aldred, J. A. Leach, K. L. Webster, M. Bierzoza

terrestrial N sources. Catchments with greater potential for hydrologic expansion had longer characteristic time constants (Creed & Band, 1998b). The N flushing concept has become the theoretical underpinning of N export models (e.g., Creed & Band, 1998a).

Further insights into catchment N export behavior can be captured in the hysteresis patterns of the relation between discharge (Q) and N concentration (C) during periods of peak N export, referred to as the C-Q relationship (Hendrickson & Krieger, 1960). Hysteresis patterns derived from the C-Q loop reveal essential insights into the hydrologic controls on biogeochemical export during a hydrologic episode (Burns et al., 2019; Heathwaite & Bierzoza, 2021). Hysteresis patterns can be classified by loop slope (positive, negative), direction (clockwise, counterclockwise), and amplitude (Figure 1) (Evans & Davies, 1998; House & Warwick, 1998). These patterns can be derived using relatively low-frequency daily measurements during major hydrologic episodes (e.g., melt/storm events) or high-frequency measurements for both major and minor hydrologic episodes (Bierzoza et al., 2023). The slope of the C-Q loop reflects whether N export is transport-limited (positive = flushing) or source-limited (negative = diluting). The direction of the C-Q loop reflects whether N sources are spatially connected and proximal to the stream (clockwise) or spatially disconnected and distal from the stream (counterclockwise). The larger the amplitude of the C-Q loop, the greater the hydrologic expansion into new terrestrial N sources (Lloyd et al., 2016). This analysis encompasses whether N export is source (supply) or transport limited, whether variable source areas are spatially organized or disorganized, and whether the hydrologic episodes expand into distal parts of the catchment or remain proximal to the catchment outlet (Burns et al., 2019). In intact forested landscapes, C-Q hysteresis patterns vary among catchments based on catchment properties (Creed & Band, 1998b). However, more research is required to determine if hysteresis patterns within catchments vary in time due to external climatic variability/climate change factors.

There are growing uncertainties in N export behavior driven by changing climatic conditions and the intensification of the hydrologic cycle (Huntington, 2006; Koutsoyiannis, 2020), an associated shift from cooler-wetter to warmer-drier conditions, a loss of winter (Contosta et al., 2019), and a weakening of hydrologic episodes (Creed, Hwang, et al., 2015; Creed, McKnight, et al., 2015). Such transformations have significant implications for downstream waters, potentially affecting productivity and biodiversity. It is essential to verify whether established hypotheses, such as the N flushing hypothesis, still apply under these new circumstances.

To address this knowledge gap, we analyze a 38-year data set of N flushing times and C-Q hysteresis metrics (Hysteresis Index [HI], Flushing Index [FI]) during dominant spring snowmelt hydrologic episodes in the Turkey Lakes Watershed, Ontario, Canada—the same northern temperate forest where the N flushing mechanism was originally proposed. This study takes place against the backdrop of changing climatic conditions and a decline in atmospheric acidic pollutants, with evidence of N declines in precipitation beginning around 2000, though recovery in N stream exports remains variable (Webster, Leach, Hazlett, et al., 2021; Webster, Leach, Houle, et al., 2021). We examine how source areas and mechanisms of stream N exports have evolved over time in intact headwater catchments, comparing upland-dominated catchments draining directly to the outlet (C35) with those draining through a wetland before reaching the outlet (C38).

We hypothesized that hydrologic intensification is driving a lengthening of N flushing times and a lowering of FI and HI as the catchment shifts from transport-limited (faster water flow, less nutrient processing, and larger contribution of spatially-organized N sources that are proximal to the stream—“flushing”) to source-limited (slower water flow, more nutrient processing, and larger contribution of spatially-disorganized N sources that are distal to the stream—“diluting”). If hydrologic intensification is driving changes in N flushing behavior, we further hypothesized that these changes will be more prominent in catchments with relatively small hydrologic storage potential (i.e., no wetlands) than in catchments with more considerable hydrologic storage potential (i.e., with wetlands), as wetlands serve to buffer against hydrologic variability.

We aim to develop a mechanistic framework that integrates global change impacts with catchment-specific patterns of solute transport. Our study revisits and reevaluates the N flushing hypothesis in light of current hydrologic conditions, providing a conceptualization and parameterization of C-Q relationships that take into account both global and local drivers of change. Most previous studies have focused on either multi-decadal C-Q responses to large-scale drivers (Basu et al., 2022; Dupas et al., 2018; Newcomer et al., 2021) or storm event C-Q patterns of solute mobilization and delivery (Knapp et al., 2022; Li et al., 2022). By synthesizing yearly and multi-decadal events, we provide essential insights for predicting future biogeochemical trends in aquatic systems, thereby addressing a long-standing research gap.

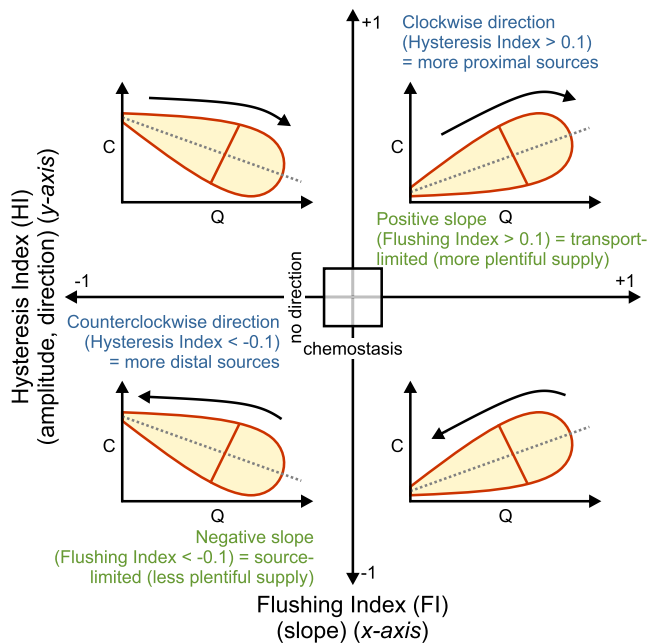


Figure 1. Graphics of hysteresis metrics derived from the concentration–discharge (C–Q) loop. For the Flushing Index (FI, x -axis), which ranges between -1 and $+1$, the *direction of slope* indicates whether solutes are transport-limited (positive = flushing) or source-limited (negative = diluting). For the Hysteresis Index (HI, y -axis), which ranges between -1 and $+1$, the *direction of the loop* indicates whether the solute sources are spatially connected and proximal to the stream (positive = clockwise) or spatially disconnected and distal from the stream (negative = counterclockwise), and the *amplitude* of HI indicates if there is smaller (narrow loop) or larger (broad loop) hydrologic expansion into new solute source areas.

2. Materials and Methods

2.1. Study Area

The Turkey Lakes Watershed (TLW; 10.5 km²) is an experimental watershed located on the Canadian Shield in the Algoma Highlands of central Ontario, Canada (47°03'N, 84°25'W, 60 km north of Sault Ste. Marie) (Figure 2) (Webster, Leach, Hazlett, et al., 2021). The TLW contains 13 actively monitored catchments that drain into a chain of lakes that ultimately empty into Batchawana Bay on the eastern shore of Lake Superior.

The TLW has a continental climate influenced by its proximity to Lake Superior. The average temperature from June 1 to May 30 from 1981 to 2020 was +4.5°C, and the average total annual precipitation was 1,215 mm. The climate shows both stationary climatic oscillations and non-stationary climate change, based on data collected from the Algoma CAPMoN (Canadian Air and Precipitation Monitoring Network) meteorological station located approximately 1.3 km southeast of the watershed (47°02'N, 84°22'W, 411 m. a.s.l.). Hereafter, “year” and “annual” refers to the June to May water year.

The TLW is predominantly covered by intact mature sugar maple (*Acer saccharum* Marsh.) forest and has a bedrock foundation with a 400 m difference in elevation from the highest point, Batchawana Mountain (644 m.a.s.l.), to its outlet at 244 m.a.s.l. Drainage patterns are controlled by major faults cut through the bedrock. The bedrock is composed of Precambrian granite and gneiss. It is overlain by a thin (≤ 2 m) till, though there are occasional deep deposits up to 65 m depth in local bedrock depressions or along fault lines (Elliot, 1985). The thin (0.5 m depth at most elevations) upper silty to sandy ablation layer of the till is relatively permeable, while the compact sandy lower basal till is relatively impermeable. Soils are orthic-ferro-humic and humo-ferric podzols, with scattered organic ferric humisol deposits in bedrock depressions and adjacent to lakes and streams. The forest soils have high nitrification rates (Foster, 1989).

In 1979, the TLW was established as a long-term monitoring site to study the effects of atmospheric acidic deposition (and recovery) on terrestrial and aquatic ecosystems (Webster, Leach, Hazlett, et al., 2021). Among the monitored headwater catchments, catchment 35 (C35) (4.47 ha) has uplands with no wetlands. In comparison, C38 (8.5 ha) features a sizable cryptic wetland (a forested swamp) covering about 20% (1.58 ha) of the catchment area (Creed et al., 2003). Snowpacks typically persist from late November/early December to late March/early April, with peak stream discharge occurring during spring snowmelt and autumn storms. The shallow soil layer and lack of significant deep groundwater inputs to streamflow in this landscape imply that streamflow solute concentrations and their correlation with discharge would be highly responsive to substantial shifts in climate and atmospheric acidic deposition over the monitoring period (Webster et al., 2022).

Catchment discharge and stream N concentrations in the stream discharge have been measured daily during snowmelt and biweekly to monthly at the catchment outlets for the calendar years 1981–2019 and water years 1982–2019. Summaries of the start-end dates, intervals, measurement locations, and sample size of catchment discharge and stream N concentrations and other input data described in the sections below are provided in Table S1 in Supporting Information S1.

2.2. Intensity of Hydrologic Cycle

This study assessed changes in the intensity of hydrologic cycling by analyzing climate-driven variations in the annual partitioning of precipitation between evapotranspiration and discharge along the Budyko curve from 1982 to 2019 (Budyko, 1974).

The Budyko curve was constructed by plotting the Evaporative Index (EI; the ratio of actual evapotranspiration [AET] to precipitation [P]) against the Dryness Index (DI; the ratio of potential evapotranspiration [PET] to P)

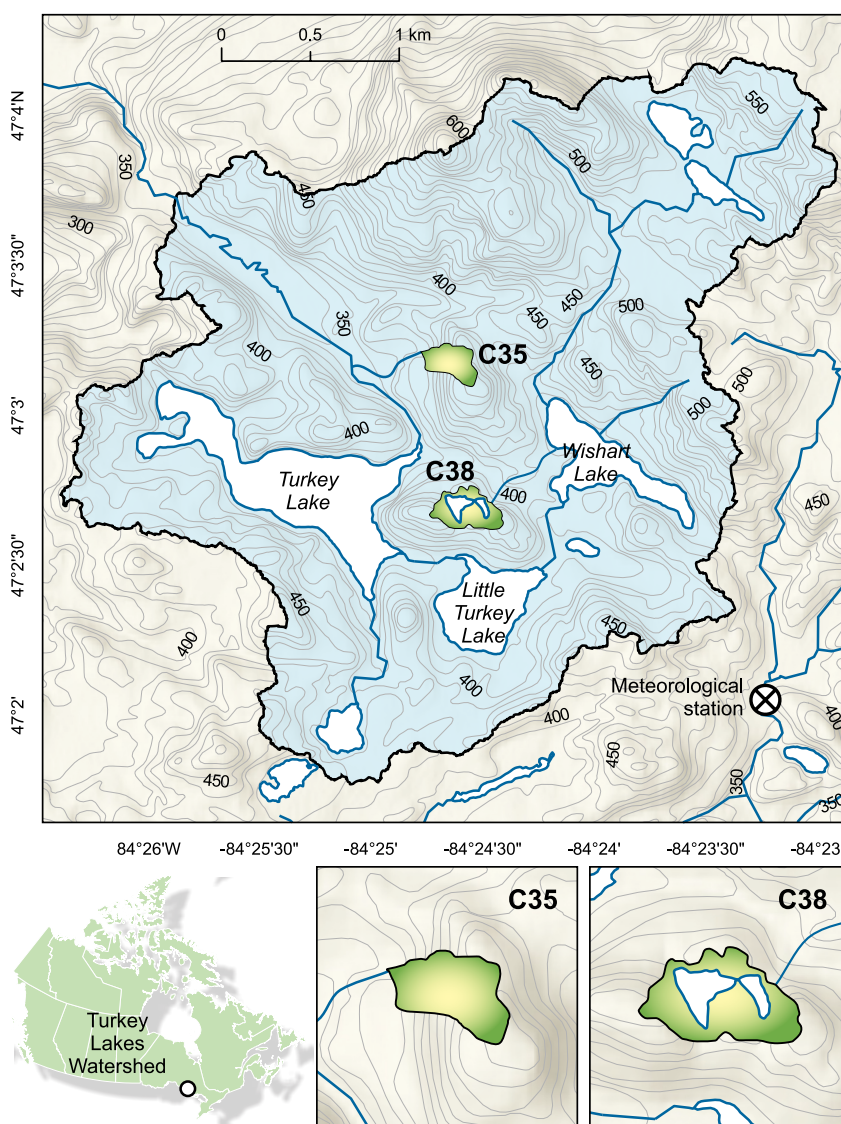


Figure 2. Map of the headwater catchments C35 and C38 in the TLW. The water flows through a chain of lakes into Norberg Creek, draining into the Batchawana River and ultimately reaching the eastern shores of Lake Superior. White polygons in C38 represent wetlands.

(Creed et al., 2014). Mean daily air temperature (T ; $^{\circ}\text{C}$) and total daily precipitation (P ; mm) were measured at the Algoma CAPMON station, and mean daily discharge (Q ; L s^{-1}) was measured at the C35 and C38 weirs. Mean monthly and annual T and total monthly and annual P and Q were calculated from daily values. Total annual PET was calculated from total monthly PET; total monthly PET (mm) was calculated from mean monthly T values using the method of Hamon (1963); the Hamon (1963) method may underestimate PET but typically performs better than other T -based PET models and about the same as radiation-based PET models (Lu et al., 2005). Total annual AET (mm) from each catchment was calculated as the difference between annual P and Q . DI was calculated as total annual PET divided by total annual P . EI was calculated for each catchment as total annual AET divided by total annual P . Approximately semi-decadal (4-year increment for 1982–1985, followed by 5-year increments from 1986 to 1990 up to 2011 to 2015, and then by a 4-year increment from 2016 to 2019) means of EI and DI were plotted against the Budyko curve to visualize intensification or de-intensification over time.

2.3. Seasons and Vegetation Responses

The snow season was defined as beginning on the first day at which snow-water equivalent (SWE) ≥ 20 mm, where 20 mm was selected to avoid transient snowpacks that develop and melt in early autumn, and ending on the first day at which SWE = 0 mm. Daily SWE (mm) was modeled using a snow accumulation and melt routine within a hydrologic model and calibrated to daily Q measurements (Leach et al., 2020). The SWE = 20 mm threshold was selected through visual comparisons of the time series of SWE and Q. Snow season total SWE accumulation was calculated as the sum of “new” daily SWE (i.e., increases in SWE from the previous day).

The growing season was determined to start on the first day when the average daily temperature remained at or above 5°C for five consecutive days, beginning on or after March 1. The season was considered to end on the first day when the minimum daily temperature fell below -2°C , on or after August. The growing season start and end days were extracted from 60-arcsecond historical monthly climate grids for North America (McKenney et al., 2011; <https://cfs.nrcan.gc.ca/projects/3/9>). Vernal windows were defined as the periods between the ends of the snow seasons and the beginnings of the growing seasons (adjusted to zero for those years where the temperature-based growing season started before the end of the snow season (3/38 years, maximum difference = 5 days) (Creed, Hwang, et al., 2015). Autumnal windows were defined as the periods between the ends of the growing seasons and the beginning of the snow seasons (Creed, Hwang, et al., 2015).

A time-integrated normalized difference vegetation index (iNDVI) for each growing season was calculated to characterize net primary productivity during the growing season (Goward et al., 1985). NDVI was calculated from Landsat Satellite Series (4–5 TM, 7 ETM+, and 8 OLI) Collection 2 Level 2 imagery from 1984 to 2019 using Google Earth Engine (GEE) using the equation:

$$\text{NDVI} = \frac{\text{NIR} - \text{Red}}{\text{NIR} + \text{Red}}$$

where NIR is the near-infrared (NIR) spectrum band (band 4 for TM and ETM+, band 5 for OLI) and Red is the red spectrum band (band 3 for TM and ETM+, band 4 for OLI). The spatial mean NDVI within each catchment was calculated for each annual growing season, where each growing season was divided into six intervals to obtain approximately monthly NDVI estimates (assuming that at least one Landsat image without cloud cover would be available in approximately monthly intervals). iNDVI represents the sum of NDVI measured at regular intervals, and was calculated using the trapezoidal rule equation (Reed et al., 1994):

$$\text{iNDVI} = \sum_{i=1}^n (\overline{\text{NDVI}}_{(i+1,i)} \times (t_{i+1} - t_i))$$

where $\overline{\text{NDVI}}_{(i+1,i)}$ represents the mean NDVI of two consecutive intervals, and t_i represents the number of days from the start of the growing season. NDVI values missing due to cloud cover or poor data quality were linearly interpolated using the “na.approx” function as part of the “zoo” package in R (version 4.3.2).

2.4. Atmospheric N Deposition and Stream N Export

Atmospheric acidic deposition for the TLW was calculated from bulk precipitation samples (i.e., a mixture of wet deposition and an unknown and variable portion of dry deposition) collected weekly from 1982 to 2016 at the Algoma CAPMON station. Bulk precipitation samples were filtered before the analysis for nitrate and ammonium concentrations at the Water Chemistry Laboratory at the Great Lakes Forestry Center in Sault Ste. Marie, and normalized per total precipitation volumes (mg L^{-1}). Total nitrogen (TN; nitrate-N + ammonium-N) was calculated, and total monthly TN deposition was calculated as the product of mean monthly TN concentration by total monthly precipitation volume. Total annual TN deposition was calculated using monthly values.

Stream N sampling was conducted at v-notch weirs at the catchment outlets daily during snowmelt and biweekly to monthly at other times of the year. Samples were taken in clean 2-L polyethylene bottles that were rinsed at least three times with stream water, followed by immersion to collect the final sample, with care taken not to disturb stream sediments during sampling. Stream N concentrations (C ; mg L^{-1}) in the stream discharge were measured within 2 weeks of collection at the Great Lakes Forestry Center, with sample integrity maintained by

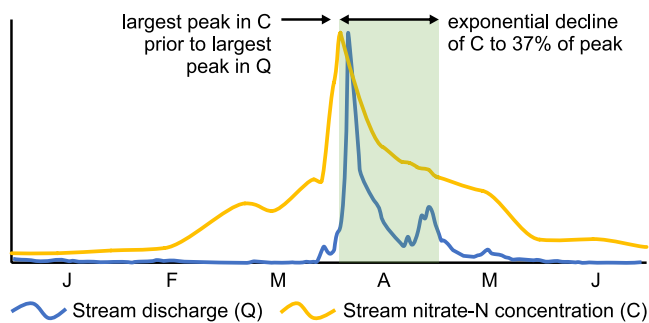


Figure 3. Schematic showing identification of spring hydrologic episode and N flushing time (time for C concentrations to decline to 37% of its peak) using annual spring time series of Q and C. The months are January (J) through June (J).

storage at 4°C in dark rooms prior to analysis at room temperature. Two daily C values in C35 were visually identified as outliers and removed (04/28/1982 and 03/06/2000). Due to equipment failures, there were no C measurements available in C38 in 1987 and 2019. Missing C values (except in 1987 and 2019 in C38) were linearly interpolated. Daily catchment N exports (kg) were calculated from daily C values and Q (L s⁻¹). Total monthly and annual catchment N exports were calculated from daily values.

2.5. N Flushing Times and C-Q Hysteresis Metrics

Spring hydrologic episodes in each year were identified from daily time series of Q and sampled (i.e., un-interpolated) C values (Figure 3). Spring hydrologic episodes were visually identified where one (or more) peaks in Q were coincident with the largest spring (February to April) peak in C (i.e., the dominant snowmelt event) followed by an apparent exponential decline in C. Peaks in Q typically occur shortly after peaks in C, but given the coarse

temporal (daily) resolution of the time series, melt events were considered valid for analysis where the Q peaks co-occurred or within ±1 day of peaks in C. Baseline Q for each dominant melt event was identified as the smallest non-zero Q value preceding any apparent peak belonging to the event, and the day of the year (DOY) of the baseline Q was identified as the start of the event. Where there was a series of days with the smallest non-zero Q value, the last DOY in the series was used. The DOY at which Q returned to the baseline value without an intermediate peak in Q or, more commonly, before which Q began to rise to another peak in another hydrologic episode was identified as the end of the event.

Within each dominant melt event, both Q and C were normalized to 0–1 values using the equation:

$$x_{i\text{-norm}} = \frac{x_i - x_{\min}}{x_{\max} - x_{\min}}$$

where x_i is the value of Q or C at time step i , x_{\max} is the maximum value of Q or C during the event, and x_{\min} is the minimum value. Visual inspection of the C-Q relationships during the dominant snowmelt events showed that all resembled loops, with Q returning approximately to baseline and C not displaying overt complexity (i.e., the loops were relatively smooth, and C did not cross the loops more than once).

N flushing time for each dominant snowmelt event was characterized by the time in days of the exponential decline of the peak C to 37% of the initial concentration per the method described by Creed and Band (1998b). Peak C was recorded for each dominant snowmelt event, and 37% of the peak C was calculated. For each snowmelt event, exponential regression coefficients were developed from sampled (i.e., un-interpolated) C as the dependent variable and DOY as the independent variable for the period beginning at the DOY of peak C and ending at the end of the snowmelt event, ensuring that a minimum of three samples were used (i.e., extending to the first DOY after the snowmelt event where there were only two samples during the event). Regression coefficients were used to model C for all days in the spring period (January to June). The day of the year at which the modeled concentration was closest to 37% of the peak concentration was recorded as the day on which the concentration had declined to 37%. The time (t) in days for the concentration to decline from the peak value was then calculated. The exponential regression coefficient and t were calculated in Microsoft Excel™ v. 2108.

Nitrogen C-Q hysteresis metrics (Hysteresis Index (HI) and Flushing Index (FI)) were calculated from daily Q and interpolated C to describe C-Q relationships using a Matlab script developed by and described in Heathwaite and Bierzoza (2021) and implemented in Matlab R2022a (MathWorks, 2022). The HI describes C change on rising and falling limbs where (a) HI < -0.1 indicates a counter-clockwise response (i.e., C on falling limb higher than on rising limb, nutrient flushing from more distal sources), (b) -0.1 < HI < +0.1 indicates a linear response (or no direction), and (c) HI > +0.1 indicates a clockwise response (i.e., C on rising limb higher than on falling limb, nutrient flushing from more proximal sources). For each 5th percentile of Q (k), HI_k was calculated as normalized C on the rising limb corresponding to Q_k minus normalized C on the falling limb corresponding to Q_k (Lloyd et al., 2016); HI at $k = 50$ (median; HI₅₀) was used to describe HI for each snowmelt event. The FI describes the relative change in C during an event where (a) FI < -0.1 indicates dilution (i.e., C decreases with Q, flushing is

source limited, more limited N supply), (b) $-0.1 < FI < +0.1$ indicates a neutral response (i.e., chemostasis), and (c) $FI > +0.1$ indicates flushing (i.e., C increases with Q, flushing is transport limited, less limited N supply). FI was calculated using the equation:

$$\begin{aligned} & \text{IF } (C_{\text{base}} \leq C_{\text{peak}}) \\ & \text{THEN } FI = C_{\text{peak}} - C_{\text{base}}/C_{\text{peak}} \\ & \text{ELSE } FI = C_{\text{peak}} - C_{\text{base}}/C_{\text{base}} \end{aligned}$$

where C is the actual non-normalized concentration, C_{base} is C at the baseline Q DOY, and C_{peak} is C at the Q peak DOY.

Semi-decadal (1982–1985, 1986 to 1990 continuing in 5-year increments up to 2011 to 2015, and 2016 to 2019) means of HI were plotted against semi-decadal means of FI to visualize expansion or contraction of variable source areas and changes in N supply over time.

2.6. Statistical Analysis

The normality of distributions of annual time series variables was assessed using the Jarque-Bera test (Jarque & Bera, 1987). After finding that most (21/23 or 91%) of the variable distributions were normal ($p > 0.05$), we generated Pearson correlation matrices in each catchment to describe the strength of relationships between annual mean T, total P, total Q, DI, EI, and climate oscillation indices, including the Atlantic Mid-decadal Oscillation (AMO, estimated period of oscillation is 70 (60–80) years), Pacific Decadal Oscillation (PDO, estimated period of oscillation is 25 (20–30) years), El Niño and La Niña (El Niño-Southern Oscillation) (ENSO, estimated period of oscillation is 2–7 years), and North Atlantic Oscillation (NAO, estimated period of few days to few months). We obtained monthly climate oscillation data from the Monthly Atmospheric and Ocean Time Series at NOAA Physical Sciences Laboratory Climate Indices (<https://psl.noaa.gov/data/climateindices/>) and aggregated it to annual totals. We conducted Jarque-Bera tests and generated Pearson correlation matrices using Microsoft Excel™ version 2108.

Annual trends in the time series of N export, T, P, Q, DI, EI, TN deposition flux, lengths of snow and growing seasons and vernal and autumnal windows, SWE accumulation, previous growing season iNDVI, climate oscillation indices, hysteresis metrics, and flushing times were assessed using Mann-Kendall and Sen's slope tests in R (“trend” and “Kendall” packages), where Mann-Kendall was used to detect significant ($p < 0.1$) trends and Sen's slope was used to determine the direction of the trend (positive or negative). Monthly trends in the same time series T, P, and DI in TLW and Q and EI in C35 and C38 were assessed using the seasonal trend decomposition after LOESS smoothing (Cleveland et al., 1990) using the “stl” function in R.

Random forest analyses were used to evaluate the relative importance of selected explanatory variables on N export in each catchment. Explanatory variables were selected based on the identification of proxies for process controls on catchment soil N accumulation, including climatic explanatory variables (T, P, DI, EI, Q, PDO, NAO, ENSO, AMO, which were screened to remove the effects of collinearity using a Pearson correlation matrix), and N supply (atmospheric acidic deposition and iNDVI, which is a proxy for the amount of N that can be deposited on the forest floor), N storage (snow season length, which is a proxy for when forest floor litter decomposes under a snowpack but is not released in quantity to the stream), and N transport (vernal window length, which is the period when flushing occurs, and the N flushing time) (see Creed et al., 1996 for a detailed description of process controls). Random forests were constructed for both catchments using a 38×8 input data matrix, where 38 is the number of years in the time series, and 8 is the 7 explanatory variables plus the response variable (N export). Random forests were developed using 1,000 trees. Variable importance plots from 100 random forests were generated to reveal the relative importance of each potential explanatory variable. Partial dependence plots from the same 100 random forests were generated to determine the relationships between each potential explanatory variable and N export in each catchment while holding all other variables constant. Histograms of the explanatory variables were visually examined for evidence of strongly skewed distributions or outliers that could drive the extremes of the relationships. Random forest analyses were performed in R (“randomForest” package).

3. Results

3.1. Hydrologic Intensification-De-Intensification Cycle

Over the past four decades, the hydrologic cycle exhibited two distinct phases: intensification (1982–2005) and de-intensification (2006–2019). During the intensification phase, increased energy inputs led to warmer-drier periods, reducing water yields. During the de-intensification phase, decreased energy inputs led to a return to cooler-wetter periods, increasing water yields in C35 (catchment dominated by uplands with no wetlands), and restoring them in C38 (catchment with wetland covering 20% of area).

Figure 4 illustrates these trends through annual time series of T, P, SWE, and Q. Both catchments displayed a *low-frequency oscillation* (multi-decadal) between the climatic extremes. Superimposed on this low-frequency oscillation was a *higher-frequency oscillation* (i.e., multi-annual) switching between warmer-drier and cooler-wetter climatic conditions. Notably, C35 showed a more robust recovery in Q than C38. Monthly T trends analysis revealed uniform warming or cooling across all months with no specific trend in any month. Monthly P trends showed a disruption in precipitation patterns throughout the year, concentrated in the period from February (becoming wetter) to March (becoming drier) and the period from August (becoming drier) to September (becoming wetter). Monthly Q trends showed a disruption of discharge during the months during which the most dominant snowmelt events occurred, including an increasing then decreasing trend in April in C35 and a decreasing trend in April in C38 (Figure 4).

Figure 5 further illustrates these trends. Budyko metrics—namely, EI and DI—followed a trajectory along the Budyko curve, transitioning toward the threshold between energy and water limitation ($PET/P = 1$) during hydrologic intensification (1982–2005) and then reversing during de-intensification (2006–2019). Hysteresis loops accompanied these movements: C35 returned to its initial state, whereas C38 showed incomplete recovery, indicating legacy effects of the warmer-drier conditions in the catchment with larger hydrologic storage. Throughout the entire time series, there were significant ($p < 0.1$) increases in EI in both catchments but not in DI ($p \geq 0.1$).

Table 1 illustrates the impact of multi-year climate oscillations on catchment hydrology, specifically highlighting the AMO (Atlantic Mid-decadal Oscillation, 70 year period), PDO (Pacific Decadal Oscillation, 25 year period), ENSO (El Niño and La Niña [El Niño-Southern Oscillation], 2–7 year period), and NAO (North Atlantic Oscillation, few days to few months period).

AMO and NAO had the most prominent influence on climatic patterns. AMO is associated with warmer-drier conditions, as indicated by the positive correlations for T, DI, and EI, along with negative correlations with P and Q. In contrast, NAO had the opposite effect, promoting cooler-wetter conditions, as indicated by negative correlations for T, DI, and EI, along with positive correlations for P and Q.

3.2. Seasonal and Vegetation Response Shifts

The hydrologic cycling of intensification-de-intensification had subtle effects on the length of the snow season, the vernal window, and the autumnal window. In contrast, the effects on the length of the growing season were profound (Figure 6). Intensification resulted in non-significant ($p \geq 0.1$) shortening of the snow season (later start and earlier ending), lengthening of the vernal window (earlier start), lengthening of the growing season (later ending), and shifting of the autumnal window (later start and ending) (Figure 6a). De-intensification reversed these trends, except for a continued lengthening of the growing season (Figure 6a), which coincided with a significant ($p < 0.1$) rise in iNDVI (Figure 6b).

3.3. Changes in Atmospheric N Deposition and Stream N Export

Annual atmospheric acidic deposition, which includes wet nitrate-N and ammonium-N, rose to a peak in the late 1980s before declining until the end of the data series (no data were available after 2016). This trend had notable monthly variability (Figure 7a). The increase and subsequent decrease in annual atmospheric acidic deposition were reflected in stream N exports, although there were significant spikes during the transition phase from intensification to de-intensification (Figure 7b).

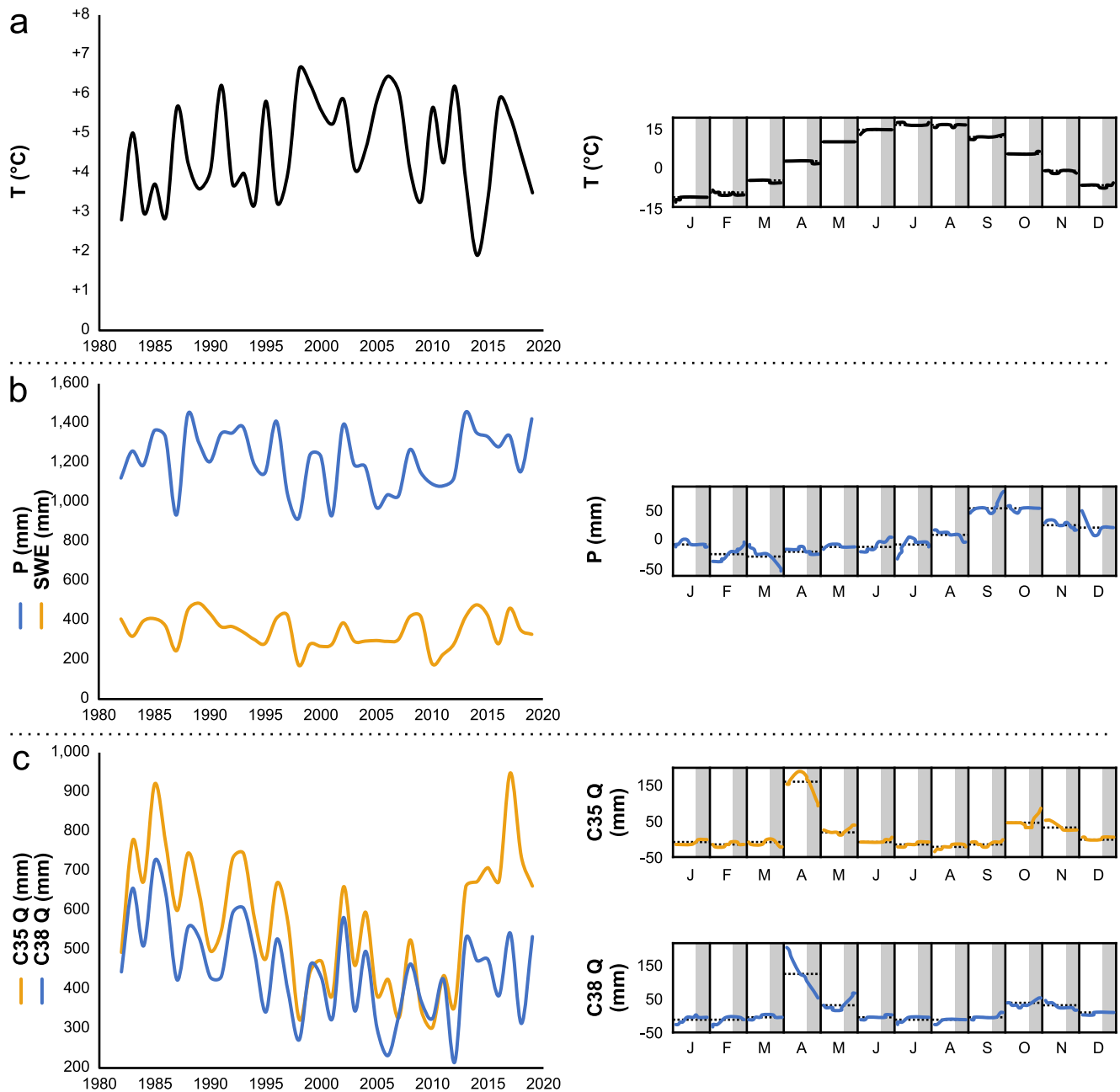


Figure 4. Annual and monthly (January [J] to December [D]) time series of: (a) mean temperature (T ; $^{\circ}\text{C}$); (b) total precipitation (P ; mm) (blue) and total snow water equivalent (SWE; mm) (orange); and (c) total discharge (Q ; mm) in C35 (orange) and C38 (blue). In the monthly time series, white boxes represent the intensification period, and gray boxes represent the de-intensification period of the hydrologic cycle over the time series.

3.4. Changes in N Flushing Times and C-Q Hysteresis Metrics

The hydrologic intensification-de-intensification cycle affected N flushing times differently in the two catchments. In catchment C35, N-flushing times increased significantly ($p < 0.1$), while they remained stable in catchment C38 (Figure 8). This divergence in N flushing behavior points to differential catchment responses to hydrologic changes. Intensification, associated with smaller N exports (Figure 7), may have allowed for an accumulation of N supply. The transition to de-intensification, associated with larger N exports (Figure 7), may have allowed access to the accumulated N supply that contributed to N export.

The C-Q hysteresis metrics (Figure 9) closely aligned with N flushing times.

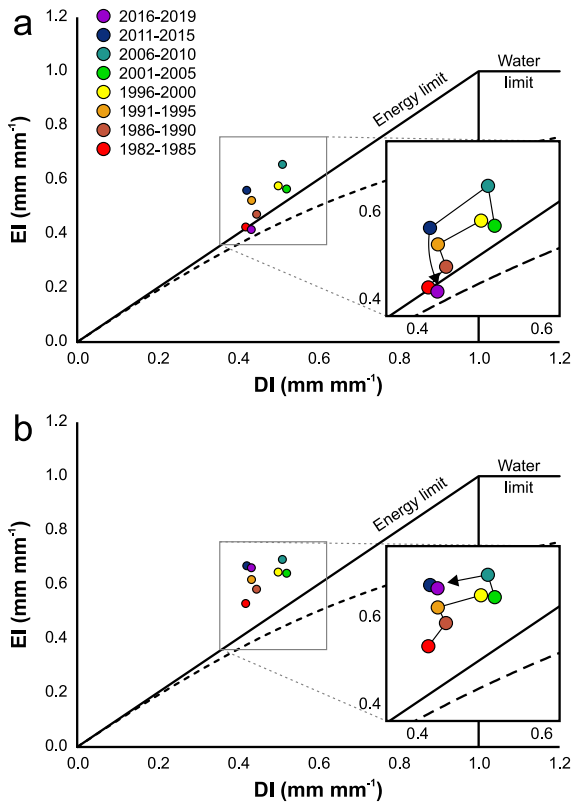


Figure 5. The intensity of the hydrologic cycle is represented on the Budyko curve by the mean semi-decadal Dryness Index (DI) and Evaporative Index (EI) values in (a) C35 and (b) C38. DI and EI increased for the first 25–30 years, shifting toward the threshold between energy- and water-limitation ($PET/P = 1$). DI and EI decreased for the last 10–15 years, returning to starting DI and EI values in C35 but not in C38. The years are color-coded to reflect a shift from warmer and drier periods (red) to cooler and wetter periods (purple).

Despite variability in DI and EI, the C-Q hysteresis metrics remained relatively stable throughout most of the time series. In both C35 and C38, the flushing index (FI) remained on the right side of the x -axis, which means flushing, as indicated by the circles that represent the 5-year averages and the lines that represent individual years within each 5-year period. However, the hysteresis index (HI) fluctuated, ranging from positive values (toward the top on the y -axis), indicating spatially-organized, proximal N sources, to near zero or negative values (toward the middle on the y -axis), indicating more spatially-disorganized, distant sources (Figure 9). In particular, a significant shift away from positive HI values occurred during the last 5 years in both catchments (purple circles), with this shift particularly evident in C35 (Figure 9a). This shift may reflect legacy effects of accumulated nitrogen during the warmer-drier conditions of preceding years. During this period, there was an escalation in chemodynamic response, coinciding with changes in N flushing times; before 1995, N flushing times were relatively short and stable but thereafter lengthened and became more variable. Some of the most extreme N flushing times were recorded toward the end of the time series (see Figure 8).

3.5. Drivers of Stream N Export

Random forest analyses identified climate, along with N supply, storage, and transport, as influential predictors of N export (Figure 10). N storage (represented by snow season length) and N transport (represented by vernal window length) emerged as the most consequential predictor variables of N export in both catchments. N export increased with lengthening snow seasons but declined as vernal windows lengthened. EI ranked as the third most significant predictor variable in both catchments, with N export decreasing as EI increased. While DI was an important predictor variable in C38, showing a similar decline in N export with increasing DI (Figure 10b), N export in C35 was unaffected by changes in DI (Figure 10a). N supply (represented by N flushing times) was an important predictor variable in C38, where longer flushing times correlated with increased N export (Figure 10b). While N flushing times did not influence N export in C35, N supply as represented by

atmospheric acidic deposition was a moderately important predictor variable in this catchment with the same positive correlation with N export (Figure 10a). Notably, N export in both catchments was unaffected by changes in N supply as indicated by previous growing season iNDVI. Histograms of these drivers showed no evidence of skewed distributions or outliers that might bias N export (Figure S1 in Supporting Information S1).

4. Discussion

The N flushing hypothesis—which was conceptualized during the 1980s—was developed during conditions of rising temperatures and atmospheric N deposition (Creed et al., 1996), but these conditions have changed. Northern temperate forests are undergoing substantial transformations due to increasing climatic variability and ongoing acidification recovery (Laudon et al., 2017). The hydrologic cycle is intensifying, with wet periods becoming wetter during spring and autumn and dry periods becoming drier during summer (Creed, Hwang, et al., 2015; Huntington, 2006; Senar et al., 2018). However, this intensification is not linear—there are fluctuations between intensification and de-intensification, with the latter becoming more prominent in the 21st century (Koutsoyiannis, 2020). This variability in the hydrologic cycle is influencing N export in forested catchments, creating uncertainty about the future productivity and biodiversity of downstream surface waters.

4.1. Intensification and De-Intensification of the Hydrologic Cycle

We hypothesized that climate-driven hydrologic intensification would increase the event Dryness Index (DI) and the Evaporative Index (EI), which, in turn, would lengthen N flushing times and shift concentration (C)-flow (C-Q) hysteresis metrics. Precisely, this would reflect a transition from “flushing”—where N sources are spatially

Table 1

Pearson Correlation Matrix Between June-May Annual Mean Temperature (T; °C), Total Precipitation (P; mm), Dryness Index (DI: Total Potential Evapotranspiration ((PET)/P); mm mm⁻¹), Evaporative Index (EI: Total Actual Evapotranspiration (AET, P-Discharge (Q)/P); mm mm⁻¹), Total Discharge (Q; mm), and Climate Oscillation Indices (AMO, ENSO, NAO, and PDO) for C35 (Top) and C38 (Bottom)

C35	T	P	DI	EI	Q	PDO	NAO	ENSO	AMO
Mean temperature (T)									
Total precipitation (P)	-0.44 (0.005)								
Dryness Index (DI = PET/P)	+0.69 (<0.001)	-0.93 (<0.001)							
Evaporative Index (EI = AET/P)	+0.32 (0.053)	-0.35 (0.032)	+0.38 (0.019)						
Total discharge (Q)	-0.43 (0.008)	+0.70 (<0.001)	-0.69 (<0.001)	-0.91 (<0.001)					
PDO	-0.22 (0.190)	-0.02 (0.892)	+0.01 (0.959)	-0.52 (0.001)	+0.39 (0.016)				
NAO	-0.16 (0.347)	+0.21 (0.213)	-0.23 (0.170)	-0.39 (0.017)	+0.36 (0.028)	+0.10 (0.553)			
ENSO	+0.25 (0.127)	-0.08 (0.636)	+0.20 (0.232)	-0.04 (0.802)	+0.00 (0.982)	+0.51 (0.001)	+0.12 (0.490)		
AMO	+0.43 (0.008)	-0.14 (0.394)	+0.27 (0.112)	+0.34 (0.037)	-0.31 (0.060)	-0.33 (0.049)	-0.43 (0.009)	-0.09 (0.599)	

C38	T	P	DI	EI	Q	PDO	NAO	ENSO	AMO
Mean temperature (T)									
Total precipitation (P)	-0.44 (0.005)								
Dryness Index (DI = PET/P)	+0.69 (<0.001)	-0.93 (<0.001)							
Evaporative Index (EI = AET/P)	+0.44 (0.006)	-0.37 (0.023)	+0.46 (0.004)						
Total discharge (Q)	-0.51 (0.001)	+0.74 (<0.001)	-0.76 (<0.001)	-0.90 (<0.001)					
PDO	-0.22 (0.190)	-0.02 (0.892)	+0.01 (0.959)	-0.33 (0.045)	+0.23 (0.170)				
NAO	-0.16 (0.347)	+0.21 (0.213)	-0.23 (0.170)	-0.18 (0.287)	+0.21 (0.203)	+0.10 (0.553)			
ENSO	+0.25 (0.127)	-0.08 (0.636)	+0.20 (0.232)	-0.00 (0.987)	-0.03 (0.841)	+0.51 (0.001)	+0.12 (0.490)		
AMO	+0.43 (0.008)	-0.14 (0.394)	+0.27 (0.112)	+0.53 (0.001)	-0.46 (0.005)	-0.33 (0.049)	-0.43 (0.009)	-0.09 (0.599)	

Pearson r	-1.00								+1.00
-----------	-------	--	--	--	--	--	--	--	-------

Note. Pearson correlations coefficients with p-values in parentheses.

organized and proximal to the stream (transport-limited)—to “diluting”—where N sources are more disorganized and distant from the stream (source-limited).

We observed hydrologic intensification between 1982 and 2005, marked by warmer-drier conditions, during which EI and DI increased, yet N flushing times and C-Q hysteresis metrics remained relatively stable. In contrast, the period from 2006 to 2019, marked by cooler-wetter conditions, shifted toward hydrologic de-intensification. During this period, EI and DI decreased, N flushing times lengthened but became more variable, and C-Q hysteresis metrics showed a small shift toward more negative (or less positive) flushing index (FI)

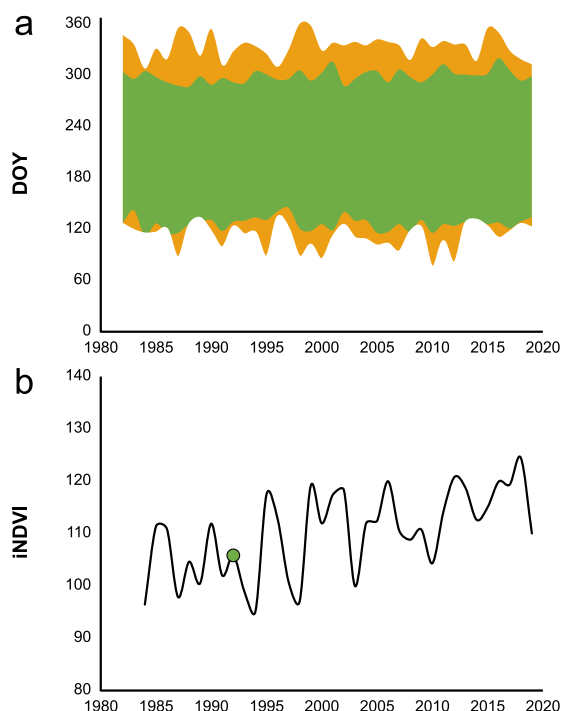


Figure 6. Annual time series of (a) snow season (white, first DOY with SWE \geq 20 mm to first DOY with SWE = 0 mm), windows (orange, vernal window = end of snow season to start of growing season; autumnal window = end of growing season to start of snow season), and growing season (green), and (b) productivity of the growing season as indicated by the integrated Normalized Difference Vegetation Index (iNDVI). There was a significant ($p < 0.1$) increase in iNDVI; the green point (1992) was missing data and therefore estimated using a linear regression of year versus iNDVI.

and a more pronounced shift toward more negative (or less positive) hysteresis index (HI) values. This transition from intensification to de-intensification was reflected differently across catchments. For example, C35 began within the Budyko curve in the 1980s, moved above it during hydrologic intensification, and returned to it as conditions de-intensified. In contrast, C38 started above the curve and stayed elevated even as EI and DI decreased, indicating that the presence of wetlands may have facilitated a greater-than-expected allocation of water to the atmosphere during de-intensification (Figure 5).

These fluctuations were influenced by both climate change and natural climate oscillations, such as the Atlantic Multidecadal Oscillation (AMO) (Table 1). The hydrologic cycle's varying intensity has implications for forested catchment processes, as described below.

4.2. Effects on N Supply

Hydrologic intensification contributes to more significant mid-winter melt events, rain-on-snow events, and more concentrated spring melts, resulting in larger N exports (Casson et al., 2011; Creed, Hwang, et al., 2015; Kurian et al., 2012).

In northern temperate forests of the northeastern U.S. and eastern Canada, the traditional “spring thaw” no longer marks the onset of spring. Over the past century, cold, snowy conditions have increasingly been replaced by an unconsolidated, mushy matrix of soil waters (Contosta et al., 2019), with significant implications for energy, water, and nutrient flows during the vernal and autumnal windows (Contosta et al., 2017). Snow is a thermal buffer that protects soil from freezing and supports microbial activity throughout winter. This microbial activity contributes to a pulse of N-rich discharge during the spring hydrologic episode (Tatariw et al., 2017). The loss of cold, snowy conditions—resulting in a thinner and shorter snow season—often leads to intensified soil freeze-thaw cycles. These cycles can reduce soil microbial

biomass and activity, lower N cycling (Sorenson et al., 2018), or cause microbial cell death and lysis. The latter can trigger an increase in N-rich discharge during the spring hydrologic episode (Sorenson et al., 2020).

The loss of cold, snowy conditions also affects the timing of leaf-on and leaf-off events, which, in turn, influence the soil N pool (Groffman et al., 2012). However, there has yet to be a consensus on this relationship's timing, magnitude, direction, or extent (Gill et al., 2015). Most studies suggest spring leaf-on occurs earlier (Crabbe et al., 2016), but autumn leaf-off varies. Some studies report earlier autumn leaf-off (Fu et al., 2014), some report no significant change (Crabbe et al., 2016), and others report delayed autumn leaf-off (Gill et al., 2015). Keenan and Richardson (2015) found that spring leaf-on and autumn leaf-off are interconnected, with earlier or later spring events influencing autumn senescence, with legacy effects on N cycling into the following year. Autumn leaf-off contributes N to the forest floor, released during the spring melt.

Canopy defoliation may also be the result of the increased frequency, intensity, and duration of native or invasive insect outbreaks (Tobin et al., 2013), redistributing soil N within forested catchments (Lovett et al., 2002) and contributes to temporary increases in N discharges (Eshleman et al., 1998; Lewis & Likens, 2007; Swank et al., 1981).

Following the period of hydrologic intensification, the forested catchments in our study responded to the subsequent hydrologic de-intensification with longer snow seasons, a narrowing of the vernal and autumnal windows, and presumed recovery of at least part of the soil N pool, as atmospheric acidic deposition continued to decline.

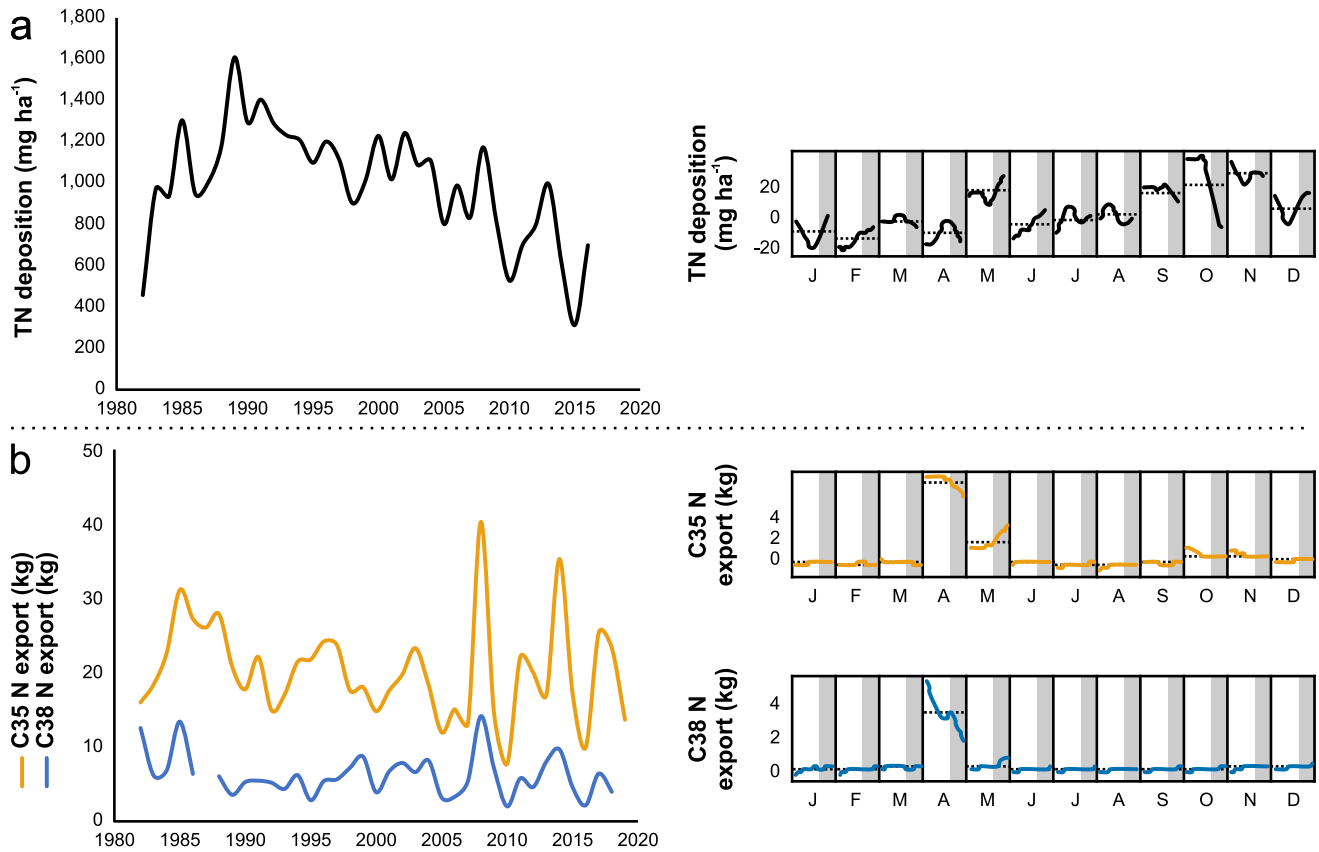


Figure 7. Annual and monthly (January [J] to December [D]) time series of (a) atmospheric total nitrogen (TN) deposition (mg ha^{-1}), and (b) stream nitrate-N export (kg) recorded at the catchment weirs in C35 (orange) and C38 (blue). In the monthly time series, white boxes represent the intensification period, and gray boxes represent the de-intensification period of the hydrologic cycle over the time series.

4.3. Effects on C-Q Relationships

We further hypothesized that catchments respond differently to hydrologic intensification versus de-intensification, with those catchments with larger hydrologic storage potential (i.e., wetlands) allowing for buffering against these hydrologic changes.

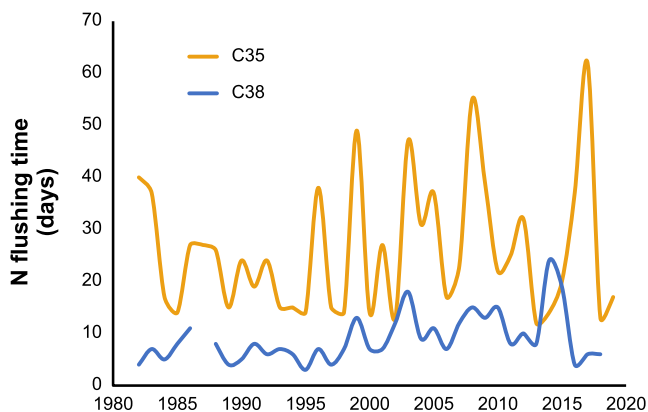


Figure 8. Annual time series of N flushing times during the peak spring hydrologic flushing episodes in C35 (orange) and C38 (blue).

The catchments exhibited different hydrological and biogeochemical responses to and recovery from hydrologic intensification. Specifically, C35 and C38 showed differing hydrological recovery patterns. For example, compared to the baseline Q in the early 1980s, Q in C35 returned to baseline conditions but not in C38 (Figure 4). This differential recovery occurred even as the forested landscape exhibited continued increases in net primary production (i.e., iNDVI) (Figure 6) despite the switch from hydrologic intensification to de-intensification. Further, C35 and C38 showed differing biogeochemical recovery patterns. For example, declines in atmospheric acidic deposition were mirrored in declines in catchment N export in both C35 and C38 until the transition from hydrologic intensification to de-intensification. At this point, substantial year-to-year variability in N export was exhibited, particularly in C35 compared to C38 (Figure 7).

Catchments can either amplify or mitigate N exports driven by climate. In C35, the absence of wetlands amplified stream N export and increased year-to-year variability in catchment N flushing times and C-Q hysteretic metrics (Figures 8 and 9). However, in C38, the presence of wetlands facilitated

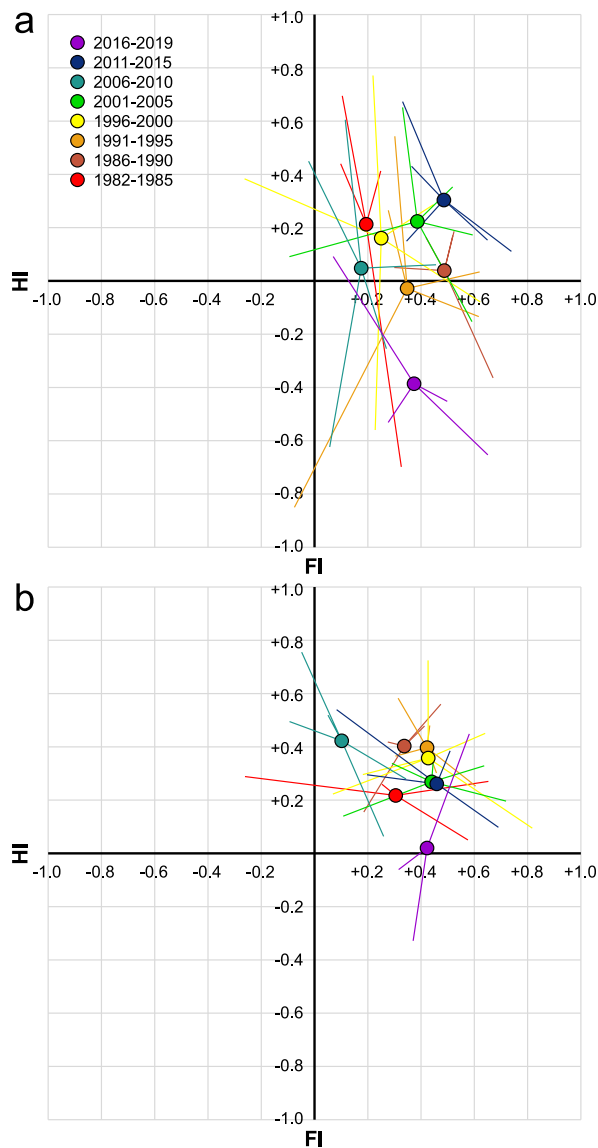


Figure 9. Plots of concentration-discharge (C-Q) hysteresis metrics (Hysteresis Index [HI] vs. Flushing Index [FI]) in (a) C35 and (b) C38. The C-Q hysteresis metrics are presented as means in 5-year increments by circles, with the individual years within the increment as lines emanating from the means. The years are color-coded to reflect a shift from warmer-drier periods (red) to cooler-wetter periods (purple).

dominance of flushing (positive FI) from proximal N sources (positive HI) (Figure 9). The stability of the C-Q patterns may have resulted from C and Q being “in sync,” with both C and Q decreasing simultaneously. However, during the subsequent period of hydrologic de-intensification, climate conditions shifted to cooler and wetter conditions in the face of ongoing declines in atmospheric acidic deposition, likely leading to unstable C-Q hysteric metrics, with the predominance of flushing (less positive to negative FI) from distal N sources (less positive to negative HI) (Figure 9). The instability of the C-Q patterns may have resulted from C and Q being “out of sync,” with C decreasing while Q is increasing. These changes indicate a shift from transport-limitation toward source-limitation and a general increase in the relative importance of hydrological over biogeochemical processes (Heathwaite & Bieroza, 2021; Thompson et al., 2011).

HI was more variable than FI, indicating that the direction and amplitude of the hysteresis loops was more unstable than the slope. The relatively large variation in HI likely reflects a major variation in the delivery of N to the

alternative fates for catchment N sources. Wetlands promote denitrification, producing nitrous oxide (N_2O) and molecular nitrogen (N_2) (Enanga et al., 2017). Denitrification in wetlands during winter (Enanga, Creed, Fairweather, & Casson, 2016) and during summer rain events (Enanga, Creed, Casson, & Beall, 2016) increased atmospheric nitrogen export and reduced aquatic nitrogen export. Consequently, in C38, wetlands mitigated stream N export and reduced year-to-year variability in catchment N flushing times and C-Q hysteresis metrics (Figures 8 and 9).

N flushing times and C-Q hysteresis metrics may also have limits regarding their resistance to change and resilience to recovery from change (Creed et al., 2014). The synergistic effects of climate trends and oscillations can induce extreme drought conditions, disrupting hydrologic connectivity between uplands, ecotones, wetlands, and streams, which in turn affects the transfer and export of energy, matter, and nutrients (Mengistu, Creed et al., 2013; Mengistu, Quick, & Creed, 2013; Senar et al., 2018). Following the Millennium Drought in Australia, catchments did not return to pre-drought conditions after the return of normal precipitation, with increased forest productivity and associated enhanced ET implicated (Petersen et al., 2021). Petersen et al. (2021) suggested that catchments might be limited to resilience to hydrologic extremes, beyond which they transition to an alternative stable state. In our study, catchments displayed varying degrees of recovery from hydrologic intensification. While the Dryness Index (DI) and Evaporative Index (EI) in catchment C35 and the DI in catchment C38 returned to pre-drought conditions, the EI in C38 remained elevated in the later years of the study period (Figure 5). Nevertheless, both C35 and C38 showed increased variation in their N flushing times and C-Q hysteresis metrics.

In previous studies of TLW catchments, McPhail et al. (2023) suggest that the C-Q relationships of stream solutes remains persistent despite influences such as climate change and acidification recovery. However, contrary to McPhail et al. (2023), our findings indicate that the C-Q relationship of stream N does not remain persistent. Instead, it shows increasing variability in C-Q hysteresis metrics, potentially reflecting a limit to resilience under hydrologic extremes.

4.4. Effects on Coupling (vs. Decoupling) of C and Q

C-Q relationships, which reflect a complex interplay between the hydrological and biogeochemical processes, change across both temporal and spatial scales (Bieroza et al., 2023; Godsey et al., 2009; McPhail et al., 2023; Thompson et al., 2011).

During the period of hydrologic intensification, climate conditions became warmer and drier, and atmospheric acidic deposition started to decline, likely leading to stable C-Q hysteresis metrics on interannual scales, with the pre-

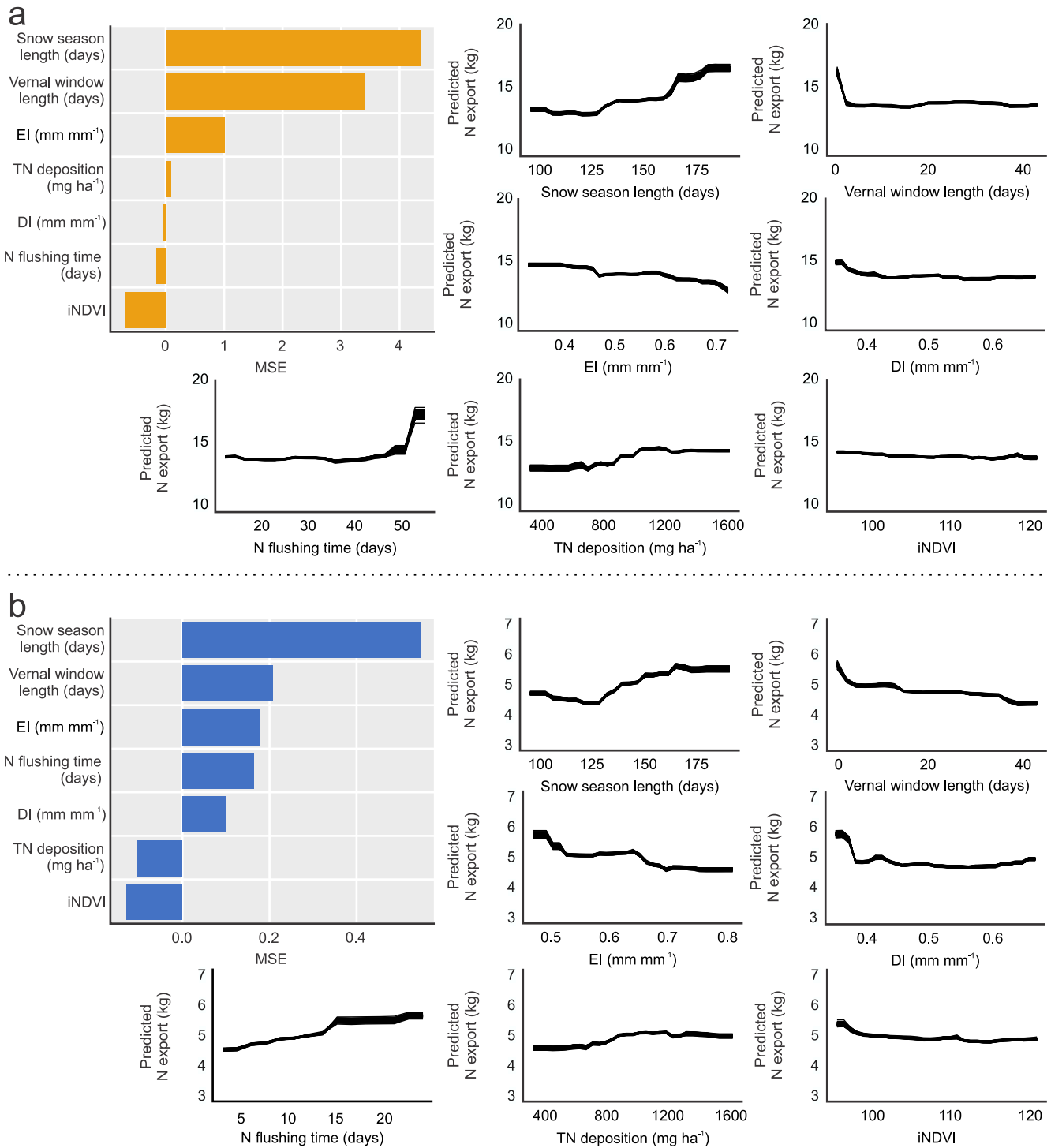


Figure 10. Results of random forest analysis of the effects of climate (Dryness Index [DI], Evaporative Index [EI]), N supply (atmospheric acidic [TN] deposition), previous growing season productivity [iNDVI], N flushing time), storage (snow season length), and transport (vernal window length) on N export using 100 random forests in (a) C35 and (b) C38. For the variable importance plots (left), the length of the horizontal bars represents the relative importance of the variable in the random forests indicated by the mean square error (MSE) (a). For the partial dependence plots (right), the mean marginal effects of each variable on N stream export while holding the other variables constant are shown.

stream. The extent of this shift was more pronounced in C35 than in C38, indicating the ability of catchments with wetlands to buffer against hydrologic change. The relatively small variation in FI reflects the more minor variation in the long-term storage and release of N from the catchments. The larger variation in HI suggests agreement with findings in previous studies; for example, Bierozza and Heathwaite (2015) showed that the direction of C-Q loops changes on a seasonal basis, from counter-clockwise during summer (hydrologic intensification, warmer and drier) to clockwise (hydrologic de-intensification, colder and wetter).

4.5. Future Research Priorities

Further research is essential to deepen our understanding of C-Q relationships under changing climate conditions. Key areas for investigation include:

1. *Temporal variability*: Examining C-Q relationships over multiple temporal scales—ranging from hours to decades—to better capture the effects of climatic variability and long-term climate change on catchment processes (McPhail et al., 2023; Rosi et al., 2022, 2023).
2. *Spatial variability*: Examining C-Q relationships across multiple spatial scales—from headwater reaches to downstream river sections—to better capture shifts in C-Q hysteresis metrics driven by transitions in hydrologic processes. These include hillslope processes, where terrestrial nutrient sources connect to streams, and riverine processes, where in-stream transformations fundamentally alter nutrient pools (Creed & Beall, 2009; Creed, McKnight, et al., 2015; Sanford et al., 2007; Taylor & Townsend, 2010).
3. *Forest dynamics*: Investigating the impacts of forest greening and browning associated with climate change on N export behavior. These shifts affect how forests partition precipitation into evapotranspiration (ET) and streamflow (Q), influence forest productivity, and ultimately alter N export dynamics (Boakye et al., 2023).
4. *Model integration*: Incorporating these insights into future models of catchment nitrogen cycling to improve predictions under changing climatic conditions.

Addressing these research priorities will enhance our understanding of how evolving climatic conditions influence hydrologic and biogeochemical processes in forested catchments.

5. Conclusions

Our study highlights the complexities of nitrate-nitrogen (N) export behavior in northern temperate forest catchments under climate change and acidification recovery. Over a multi-decadal time series, we observed significant variability in hydrologically-driven N export in two catchments, driven by climatic variability and changes in hydrologic cycling. Following hydrologic intensification, a period of hydrologic de-intensification was characterized by longer N flushing times and pronounced reductions in the Hysteresis Index (HI) in the concentration-discharge (C-Q) relationships. These changes suggest a shift from spatially-organized, proximal N sources to scattered, distal N sources. Following hydrologic intensification, larger N exports likely resulted from tapping accumulated but previously untransported N reserves. However, if these reserves are finite, future N exports may decline. The catchment with larger hydrologic storage capacity (C38) showed greater resistance to changes in the FI and HI compared to C35, emphasizing the buffering role of hydrologic storage against climatic variability. Future research will investigate whether extreme variability in N flushing times and the transition from proximal to distal N sources signal an impending tipping point.

Data Availability Statement

Data used in this study include: (a) daily stream water flow/discharge data openly available from the Government of Canada; Natural Resources Canada; CFS/GLFC/FE (2020c); (b) daily stream water concentration data openly available from the Government of Canada; Natural Resources Canada; CFS/GLFC/FE (2020b); and (c) weekly bulk precipitation chemistry (bulk deposition) data openly available from Environment and Climate Change Canada (2023). Daily snow water equivalent (SWE) data used to determine snow season start and end days, and monthly and water year annual climate (temperature, precipitation, and Hamon potential evapotranspiration) data used to support analyses are openly available from Creed et al. (2024). 60-arcsecond historical monthly climate grids for North America used to identify growing season start and end days are available on request from the Government of Canada; Natural Resources Canada; CFS/GLFC/FE (2020a). Version 2108 of Microsoft Excel™ (Microsoft Corporation, 2024) was used for data archiving and sorting, most statistical analyses, and generating

preliminary plots. Version 4.3.2 of R (R Core Team, 2023) was used to evaluate annual trends (“trend” and “Kendall” packages), monthly trends using seasonal trend decomposition (“stl” function; Cleveland et al., 1990), and random forest analyses (“randomForest” package). Calculations of HI and FI were performed using a script executed in Matlab R2022a (MathWorks, 2022) openly available from Bieroza and Creed (2024). NDVI were extracted from Landsat Collection 2 Level 2 data in Google Earth Engine using a code openly available from Bansal and Ma (2024).

Acknowledgments

The authors would like to acknowledge the work of those visionaries who established the Turkey Lakes experimental watershed, including Dean Jeffries, Ian Morrison, and John Kelso, who were not only research leaders but who enabled generations of scientists to follow them. This work is only possible with crucial funding from Environment & Climate Change Canada, Natural Resources Canada, Fisheries & Oceans Canada, and myriad other funding sources for researchers working within the watershed over the years. IFC acknowledges support from NSERC DG Grant 05265-2019 for financial support for research that led to this paper.

References

- Bansal, S., & Ma, S. (2024). NDVI extraction from landsat collection 2 Level 2 data in google Earth engine [Software]. <https://code.earthengine.google.com/bc032754e97bf4dbcdc24cc46cebb79a>
- Basu, N. B., Van Meter, K. J., Byrnes, D. K., Van Cappellen, P., Brouwer, R., Jacobsen, B. H., et al. (2022). Managing nitrogen legacies to accelerate water quality improvement. *Nature Geoscience*, *15*(2), 97–105. <https://doi.org/10.1038/s41561-021-00889-9>
- Bieroza, M., Acharya, S., Benisch, J., ter Borg, R. N., Hallberg, L., Negri, C., et al. (2023). Advances in catchment science, hydrochemistry and aquatic ecology enabled by high-frequency water quality measurements. *Environmental Science and Technology*, *57*(12), 4701–4719. <https://doi.org/10.1021/acs.est.2c07798>
- Bieroza, M., & Creed, I. F. (2024). C-Q hysteresis metrics [Software]. <https://doi.org/10.5281/zenodo.13134275>
- Bieroza, M. Z., & Heathwaite, A. L. (2015). Seasonal variation in phosphorus concentration-discharge hysteresis inferred from high-frequency in situ monitoring. *Journal of Hydrology*, *524*, 333–347. <https://doi.org/10.1016/j.jhydrol.2015.02.036>
- Boakye, E. A., Bergeron, Y., Drobyshev, I., Beekharry, A., Voyer, D., Achim, A., et al. (2023). Recent decline in sugar maple (*Acer saccharum* Marsh.) growth extends to the northern parts of its distribution range in Easter Canada. *Forest Ecology and Management*, *545*, 121304. <https://doi.org/10.1016/j.foreco.2023.121304>
- Boyer, E. W., Hornberger, G. M., Bencala, K. E., & McKnight, D. M. (1998). Response characteristics of DOC flushing in an alpine catchment. *Hydrological Processes*, *11*(12), 1635–1647. [https://doi.org/10.1002/\(SICI\)1099-1085\(19971015\)11:12%3C1635::AID-HYP494%3E3.0.CO;2-H](https://doi.org/10.1002/(SICI)1099-1085(19971015)11:12%3C1635::AID-HYP494%3E3.0.CO;2-H)
- Budyko, M. I. (1974). *Climate and life*. Academic Press.
- Burns, D. A., Pellerin, B. A., Miller, M. P., Capel, P. D., Tesoriero, A. J., & Duncan, J. M. (2019). Monitoring the riverine pulse: Applying high-frequency nitrate data to advance integrative understanding of biogeochemical and hydrological processes. *WIREs Water*, *6*(4), e1348. <https://doi.org/10.1002/wat2.1348>
- Casson, N. J., Eimers, M. C., & Watmough, S. A. (2011). Impact of winter warming on the timing of nutrient export from forested catchments. *Hydrological Processes*, *26*(17), 2546–2554. <https://doi.org/10.1002/hyp.8461>
- Cirmo, C., & McDonnell, J. (1997). Linking the hydrologic and biogeochemical controls of nitrogen transport in near-stream zones of temperate-forested catchments: A review. *Journal of Hydrology*, *199*(1–2), 88–120. [https://doi.org/10.1016/S0022-1694\(96\)03286-6](https://doi.org/10.1016/S0022-1694(96)03286-6)
- Cleveland, R. B., Cleveland, W. S., McRae, J. E., & Terpenning, I. (1990). STL: A seasonal-trend decomposition procedure based on loess. *Journal of Official Statistics*, *6*(1), 3–73.
- Contosta, A. R., Adolph, A., Burchsted, D., Burakowski, E., Green, M., Guerra, D., et al. (2017). A longer vernal window: The role of winter coldness and snowpack in driving spring transitions and lags. *Global Change Biology*, *23*(4), 1610–1625. <https://doi.org/10.1111/gcb.13517>
- Contosta, A. R., Casson, N. J., Garlick, S., Nelson, S. J., Ayres, M. P., Burakowski, E. A., et al. (2019). Northern forest winters have lost cold, snowy conditions that are important for ecosystems and human communities. *Ecological Applications*, *29*(7), e01974. <https://doi.org/10.1002/eap.1974>
- Crabbe, R. A., Dash, J., Rodriguez-Galiano, V. F., Janous, D., Pavelka, M., & Marek, M. V. (2016). Extreme warm temperatures alter forest phenology and productivity in Europe. *Science of the Total Environment*, *563–564*, 486–495. <https://doi.org/10.1016/j.scitotenv.2016.04.124>
- Creed, I. F., & Band, L. E. (1998a). Exploring functional similarity in the export of nitrate-N from forested catchments: A mechanistic modeling approach. *Water Resources Research*, *34*(11), 3079–3093. <https://doi.org/10.1029/98WR02102>
- Creed, I. F., & Band, L. E. (1998b). Export of nitrogen from catchments within a temperate forest: Evidence for a unifying mechanism regulated by variable source area dynamics. *Water Resources Research*, *34*(11), 3105–3120. <https://doi.org/10.1029/98WR01924>
- Creed, I. F., Band, L. E., Foster, N. W., Morrison, I. K., Nicolson, J. A., Semkin, R. S., & Jeffries, D. S. (1996). Regulation of nitrate-N release from temperate forests: A test of the N flushing hypothesis. *Water Resources Research*, *32*(11), 3337–3354. <https://doi.org/10.1029/96WR02399>
- Creed, I. F., & Beall, F. D. (2009). Distributed topographic indicators for predicting nitrogen export from headwater catchments. *Water Resources Research*, *45*(10), W10407. <https://doi.org/10.1029/2008WR007285>
- Creed, I. F., Hwang, T., Lutz, B., & Way, D. (2015). Climate warming causes intensification of the hydrological cycle, resulting in changes to the vernal and autumnal windows in a northern temperate forest. *Hydrological Processes*, *29*(16), 3519–3534. <https://doi.org/10.1002/hyp.10450>
- Creed, I. F., Leach, J., & Webster, K. (2024). Cycles in hydrologic intensification and de-intensification create instabilities in spring nitrate-N export C-Q behavior in northern temperate forests [Dataset]. <https://doi.org/10.5281/zenodo.13127717>
- Creed, I. F., McKnight, D. M., Pellerin, B., Green, M. B., Bergamaschi, B., Aiken, G., et al. (2015). The river as a chemostat: Fresh perspectives on dissolved organic matter flowing down the river continuum. *Canadian Journal of Fisheries and Aquatic Sciences*, *72*(8), 1272–1285. <https://doi.org/10.1139/cjfas-2014-0400>
- Creed, I. F., Sanford, S. E., Beall, F. D., Molot, L. A., & Dillon, P. J. (2003). Cryptic wetlands: Integrating hidden wetlands in regression models of the export of dissolved organic carbon from forested landscapes. *Hydrological Processes*, *17*(18), 3629–3648. <https://doi.org/10.1002/hyp.1357>
- Creed, I. F., Spargo, A. T., Jones, J. A., Buttle, J. M., Adams, M. B., Beall, F. D., et al. (2014). Changing forest water yields in response to climate warming: Results from long-term experimental watershed sites across North America. *Global Change Biology*, *20*(10), 3191–3208. <https://doi.org/10.1111/gcb.12615>
- Dupas, R., Minaudo, C., Gruau, G., Ruiz, L., & Gascuel-Oudou, C. (2018). Multidecadal trajectory of riverine nitrogen and phosphorus dynamics in rural catchments. *Water Resources Research*, *54*(8), 5327–5340. <https://doi.org/10.1029/2018wr022905>
- Elliott, H. (1985). Geophysical survey to determine overburden thickness in selected areas within the Turkey Lakes Basin, Algoma District, Ontario. In *National hydrology Research Institute Unpublished Report Series* (p. 4).

- Enanga, E. M., Casson, N. J., Fairweather, T. A., & Creed, I. F. (2017). Nitrous oxide and dinitrogen: The missing flux in nitrogen budgets of forested catchments? *Environmental Science & Technology*, *51*(11), 6036–6043. <https://doi.org/10.1021/acs.est.6b03728>
- Enanga, E. M., Creed, I. F., Casson, N. J., & Beall, F. (2016). Summer storms trigger soil N₂O efflux episodes in forested catchments. *Journal of Geophysical Research: Biogeosciences*, *121*(1), 95–108. <https://doi.org/10.1002/2015JG003027>
- Enanga, E. M., Creed, I. F., Fairweather, T., & Casson, N. J. (2016). Snow-covered soils produce N₂O that is lost from forested catchments. *Journal of Geophysical Research: Biogeosciences*, *121*(9), 2356–2368. <https://doi.org/10.1002/2016JG003411>
- Environment and Climate Change Canada. (2023). TLW-Open-Precip-ChemistryQuantity-ChimieQuantite-1981-2019-EN-FR.csv [Dataset]. *Environment and Climate Change Canada*. Retrieved from <https://data-donnees.az.ec.gc.ca/api/file?path=%2Fsubstances%2Fmonitor%2Fthe-turkey-lakes-watershed-study%2Fprecipitation-turkey-lakes-watershed-study%2FTLW-Open-Precip-ChemistryQuantity-ChimieQuantite-1981-2019-EN-FR.csv>
- Eshleman, K. N., Morgan, R. P., Webb, J. R., Deviney, F. A., & Galloway, J. N. (1998). Temporal patterns of nitrogen leakage from mid-Appalachian forested watersheds: Role of insect defoliation. *Water Resources Research*, *34*(8), 2005–2016. <https://doi.org/10.1029/98WR01198>
- Evans, C., & Davies, T. D. (1998). Causes of concentration/discharge hysteresis and its potential as a tool for analysis of episode hydrochemistry. *Water Resources Research*, *34*(1), 129–137. <https://doi.org/10.1029/97WR01881>
- Foster, N. W. (1989). Influences of seasonal temperature on nitrogen and sulfur mineralization/immobilization in a maple-birch forest floor in central Ontario. *Canadian Journal of Soil Science*, *69*(3), 501–514. <https://doi.org/10.4141/cjss89-052>
- Fu, Y. S. H., Campioli, M., Vitasse, Y., De Boek, H. J., Van den Berge, J., AbdElgawad, H., et al. (2014). Variation in leaf flushing date influences autumnal senescence and next year's flushing date in two temperate tree species. *Proceedings of the National Academy of Sciences of the United States of America*, *111*(20), 7355–7360. <https://doi.org/10.1073/pnas.1321727111>
- Gill, A. L., Gallinat, A. S., Sanders-DeMott, R., Rigden, A. J., Short Gianotti, D. J., Mantooth, J. A., & Templer, P. H. (2015). Changes in autumn senescence in northern hemisphere deciduous trees: A meta-analysis of autumn phenology studies. *Annals of Botany*, *116*(6), 875–888. <https://doi.org/10.1093/aob/mcv055>
- Gilliam, F. S., Burns, D. A., Driscoll, C. T., Frey, S. D., Lovett, G. M., & Watmough, S. A. (2019). Decreased atmospheric nitrogen deposition in eastern North America: Predicted responses of forest ecosystems. *Environmental Pollution*, *244*, 560–574. <https://doi.org/10.1016/j.envpol.2018.09.135>
- Godsey, S. E., Kirchner, J. W., & Clow, D. W. (2009). Concentration-discharge relationships reflect chemostatic characteristics of US catchments. *Hydrological Processes*, *23*(13), 1844–1864. <https://doi.org/10.1002/hyp.7315>
- Government of Canada; Natural Resources Canada; CFS/GLFC/FE. (2020a). Regional, National and International Climate Modeling, other bioclimatic variables [Dataset]. *Government of Canada; Natural Resources Canada; CFS/GLFC/FE*. Retrieved from <https://cfs.nrcan.gc.ca/projects/3/9>
- Government of Canada; Natural Resources Canada; CFS/GLFC/FE. (2020b). Turkey lakes watershed—Stream water chemistry [Dataset]. *Government of Canada; Natural Resources Canada; CFS/GLFC/FE*. Retrieved from <https://open.canada.ca/data/en/dataset/81a47b60-f5d6-47fd-9861-20c3eb10c91e>
- Government of Canada; Natural Resources Canada; CFS/GLFC/FE. (2020c). Turkey lakes watershed—Stream water flow [Dataset]. *Government of Canada; Natural Resources Canada; CFS/GLFC/FE*. Retrieved from <https://open.canada.ca/data/en/dataset/383754a1-3a37-472c-a416-30868d209e96>
- Goward, S. N., Tucker, C. J., & Dye, D. G. (1985). North American vegetation patterns observed with the NOAA-7 advanced very high resolution radiometer. *Vegetatio*, *64*(1), 3–14. <https://doi.org/10.1007/BF00033449>
- Groffman, P. M., Rustad, L. E., Templer, P. H., Campbell, J. L., Christenson, L. M., Lany, N. K., et al. (2012). Long-term integrated studies show complex and surprising effects of climate change in the northern hardwood forest. *BioScience*, *62*(12), 1056–1066. <https://doi.org/10.1525/bio.2012.62.12.7>
- Hamon, W. R. (1963). Computation of direct runoff amounts from storm rainfall. *International Association of Scientific Hydrological Publication*, *63*, 52–62.
- Heathwaite, A. L., & Bieroza, M. (2021). Fingerprinting hydrological and biogeochemical drivers of freshwater quality. *Hydrological Processes*, *35*(1), e13973. <https://doi.org/10.1002/hyp.13973>
- Hendrickson, G. E., & Krieger, R. A. (1960). Relationship of chemical quality of water to stream discharge in Kentucky. In *Proceedings of 21st International Geological Congress, Copenhagen, Denmark* (Vol. 1, pp. 66–75).
- House, W. A., & Warwick, M. S. (1998). Hysteresis of the solute concentration/discharge relationship in rivers during storms. *Water Research*, *32*(8), 2279–2290. [https://doi.org/10.1016/S0043-1354\(97\)00473-9](https://doi.org/10.1016/S0043-1354(97)00473-9)
- Huntington, T. G. (2006). Evidence for intensification of the global water cycle: Review and synthesis. *Journal of Hydrology*, *319*(1), 83–95. <https://doi.org/10.1016/j.jhydrol.2005.07.003>
- Jarque, C. M., & Bera, A. K. (1987). A test for normality of observations and regression residuals. *International Statistical Review*, *55*(2), 163–172. <https://doi.org/10.2307/1403192>
- Keenan, T. F., & Richardson, A. D. (2015). The timing of autumn senescence is affected by the timing of spring phenology: Implications for predictive models. *Global Change Biology*, *21*(7), 2634–2641. <https://doi.org/10.1111/gcb.12890>
- Knapp, J. L. A., L., i. L., & Musolff, A. (2022). Hydrologic connectivity and source heterogeneity control concentration-discharge relationships. *Hydrological Processes*, *36*(9), e14683. <https://doi.org/10.1002/hyp.14683>
- Koutsoyiannis, D. (2020). Revising global hydrological cycle: Is it intensifying? *Hydrology and Earth System Sciences*, *24*(8), 3899–3932. <https://doi.org/10.5194/hess-24-3899-2020>
- Kurian, L. M., Lautz, L. K., & Mitchell, M. J. (2012). Winter hydrology and NO₃- concentrations in a forested watershed: A detailed field study in the Adirondack Mountains of New York. *Journal of the American Water Resources*, *49*(2), 264–283. <https://doi.org/10.1111/jawr.12012>
- Laudon, H., Spence, C., Buttle, J., Carey, S. K., McDonnell, J. J., McNamara, J. P., et al. (2017). Save northern high-latitude catchments. *Nature Geoscience*, *10*(5), 324–325. <https://doi.org/10.1038/ngeo2947>
- Leach, J. A., Buttle, J. M., Webster, K. L., Hazlett, P. W., & Jeffries, D. S. (2020). Travel times for snowmelt-dominated headwater catchments: Influences of wetlands and forest harvesting, and linkages to stream water quality. *Hydrological Processes*, *34*(10), 2154–2175. <https://doi.org/10.1002/hyp.13746>
- Lewis, G. P., & Likens, G. E. (2007). Changes in stream chemistry associated with insect defoliation in a Pennsylvania hemlock-hardwoods forest. *Forest Ecology and Management*, *238*(1–3), 199–211. <https://doi.org/10.1016/j.foreco.2006.10.013>
- Li, L., Knapp, J. L. A., Lintern, A., Ng, G. H. C., Perdrial, J., Sullivan, P. L., & Zhi, W. (2024). River water quality shaped by land-river connectivity in a changing climate. *Nature Climate Change*, *14*(3), 225–237. <https://doi.org/10.1038/s41558-023-01923-x>

- Li, X., Wang, J., Lin, J., Yin, W., Shi, Y. Y., Wang, L., et al. (2022). Hysteresis analysis reveals dissolved carbon concentration—Discharge relationships during and between storm events. *Water Research*, 226, 119220. <https://doi.org/10.1016/j.watres.2022.119220>
- Lloyd, C. E. M., Freer, J. E., Johns, P. J., & Collins, A. L. (2016). Testing an improved index for analysing storm discharge-concentration hysteresis. *Hydrology and Earth System Sciences*, 20(2), 625–632. <https://doi.org/10.5194/hess-20-625-2016>
- Lovett, G. M., Christenson, L. M., Groffman, P. M., Jones, C. G., Hart, J. E., & Mitchell, M. J. (2002). Insect defoliation and nitrogen cycling in forests: Laboratory, plot, and watershed studies indicate that most of the nitrogen released from forest foliage as a result of defoliation by insects is redistributed within the ecosystem, whereas only a small fraction of nitrogen is lost by leaching. *BioScience*, 52(4), 335–341. [https://doi.org/10.1641/0006-3568\(2002\)052\[0335:IDANCI\]2.0.CO;2](https://doi.org/10.1641/0006-3568(2002)052[0335:IDANCI]2.0.CO;2)
- Lu, J., Sun, G., McNulty, S. G., & Amataya, D. M. (2005). A comparison of six potential evapotranspiration methods for regional use in the southeastern United States. *Journal of the American Water Resources Association*, 41(3), 621–633. <https://doi.org/10.1111/j.1752-1688.2005.tb03759.x>
- MathWorks. (2022). Matlab R2022a. March 15, 2022 release (version 2022a) [Software]. *MathWorks*. Retrieved from https://www.mathworks.com/products/new_products/release2022b.html
- McKenney, D. W., Hutchinson, M. F., Papadopol, P., Lawrence, K., Pedlar, J., Campbell, K., et al. (2011). Customized spatial climate models for North America. *Bulletin of the American Meteorological Society*, 92(12), 1612–1622. <https://doi.org/10.1175/2011BAMS1312.1>
- McPhail, S., Buttle, J. M., Webster, K. L., & Leach, J. A. (2023). Persistent chemostatic behaviour of stream solutes in a northern hardwood forest under climatic and atmospheric deposition changes. *Hydrological Processes*, 37(5), e14888. <https://doi.org/10.1002/hyp.14888>
- Mengistu, S. G., Creed, I. F., Kulperger, R. J., & Quick, C. G. (2013). Russian nesting dolls effect—using wavelet analysis to reveal non-stationary and nested stationary signals in water yield from catchments on a northern forested landscape. *Hydrological Processes*, 27(5), 669–686. <https://doi.org/10.1002/hyp.9552>
- Mengistu, S. G., Quick, C. G., & Creed, I. F. (2013). Nutrient export from catchments on forested landscapes reveals complex nonstationary and stationary climate signals. *Water Resources Research*, 49(6), 3863–3880. <https://doi.org/10.1002/wrcr.20302>
- Microsoft Corporation. (2024). Microsoft Excel™: April 9, 2024 release (version 2108) [Software]. *Microsoft Corporation*. Retrieved from <https://learn.microsoft.com/en-us/office/ltscc/2021/overview>
- Milly, P. C. D., Betancourt, J., Falkenmark, M., Hirsch, R. M., Kundzewicz, Z. W., Lettenmaier, D. P., & Stouffer, R. J. (2008). Stationarity is dead: Whither water management? *Science*, 319(5863), 573–574. <https://doi.org/10.1126/science.1151915>
- Newcomer, M. E., Bouskill, N. J., Wainwright, H., Maavara, T., Arora, B., Siirila-Woodburn, E. R., et al. (2021). Hysteresis patterns of watershed nitrogen retention and loss over the past 50 years in United States hydrological basins. *Global Biogeochemical Cycles*, 35(4), e2020GB006777. <https://doi.org/10.1029/2020gb006777>
- Petersen, T. J., Saft, M., Peel, M. C., & John, A. (2021). Watersheds may not recover from drought. *Science*, 372(6543), 745–749. <https://doi.org/10.1126/science.abd5085>
- R Core Team. (2023). R: A language and environment for statistical computing. October 31, 2023 release (version 4.3.2) [Software]. *R Core Team*. Retrieved from <https://www.R-project.org>
- Reed, B. C., Brown, J. F., Vanderzee, D., Loveland, T. R., Merchant, J. W., & Ohlen, D. O. (1994). Measuring phenological variability from satellite imagery. *Journal of Vegetation Science*, 5(5), 703–714. <https://doi.org/10.2307/3235884>
- Rosi, E. J., Berhardt, E. S., Creed, I. F., Likens, G. E., & McDowell, W. H. (2023). Taking the pulse of global change with World Heritage data sets. *Eos*, 104(10), 14–17. <https://doi.org/10.1029/2023eo230195>
- Rosi, E. J., Bernhardt, E. S., Solomon, C. T., Likens, G. E., McDowell, W. H., & Creed, I. F. (2022). Give long-term datasets World Heritage status. *Science*, 378(6625), 1180–1181. <https://doi.org/10.1126/science.adg0508>
- Sanford, S. E., Creed, I. F., Tague, C. L., Beall, F. D., & Buttle, J. M. (2007). Scale-dependence of natural variability of flow regimes in a forested landscape. *Water Resources Research*, 43(8), W08414. <https://doi.org/10.1029/2006WR005299>
- Senar, O. E., Creed, I. F., & Webster, K. L. (2018). Catchment-scale shifts in the magnitude and partitioning of carbon export in response to changing hydrologic connectivity in a northern hardwood forest. *Journal of Geophysical Research: Biogeosciences*, 123(8), 2337–2352. <https://doi.org/10.1029/2018JG004468>
- Sorenson, P. O., Beller, H. R., Bill, M., Bouskill, N. J., Hubbard, S. S., Karaoz, U., et al. (2020). The snowmelt niche differentiates three microbial life strategies that influence soil nitrogen availability during and after winter. *Frontiers in Microbiology*, 11. <https://doi.org/10.3389/fmicb.2020.00871>
- Sorenson, P. O., Finizi, A. C., Giasson, M.-A., Reinmann, A. B., Sanders-DeMott, R., & Templer, P. H. (2018). Winter soil freeze-thaw cycles lead to reductions in soil microbial biomass and activity not compensated for by soil warming. *Soil Biology and Biochemistry*, 116, 39–47. <https://doi.org/10.1016/j.soilbio.2017.09.026>
- Swank, W. T., Waide, J. B., Crossley, D. A., & Todd, R. L. (1981). Insect defoliation enhances nitrate export from forest ecosystems. *Oecologia*, 51(3), 297–299. <https://doi.org/10.1007/BF00540897>
- Tatarw, C., Patel, K., MacRae, J. D., & Fernandez, I. J. (2017). Snowpack loss promotes soil freezing and concrete frost formation in a northeastern temperate softwoods stand. *Winter Ecology*, 24(sp7), B42–B54. <https://doi.org/10.1656/045.024.s707>
- Taylor, P., & Townsend, A. (2010). Stoichiometric control of organic carbon-nitrate relationships from soils to the sea. *Nature*, 464(7292), 1178–1181. <https://doi.org/10.1038/nature08985>
- Thompson, S. E., Basu, N. B., Lascurain, J., Aubeneau, A., & Rao, P. S. C. (2011). Relative dominance of hydrologic versus biogeochemical factors on solute export across impact gradients. *Water Resources Research*, 47(10). <https://doi.org/10.1029/2010WR009605>
- Tobin, P. C., Parry, D., & Aukema, B. H. (2013). The influence of climate change on insect invasions in temperate forest ecosystems. In *Forestry Sciences, Challenges and opportunities for the World's Forests in the 21st century* (Vol. 81, pp. 267–293). Springer Netherlands. https://doi.org/10.1007/978-94-007-7076-8_12
- van Vliet, M. T. H., Thorslund, J., Strokai, M., Hofstra, N., Flörke, M., Macedo, H. E., et al. (2023). Global river water quality under climate change and hydroclimatic extremes. *Nature Reviews Earth & Environment*, 4(10), 687–702. <https://doi.org/10.1038/s43017-023-00472-3>
- Webster, K., Leach, J. A., Hazlett, P. W., Fleming, R. L., Emilson, E. J. S., Houle, D., et al. (2021). Turkey lakes watershed, Ontario, Canada: 40 years of interdisciplinary whole-ecosystem research. *Hydrological Processes*, 35(4), e14109. <https://doi.org/10.1002/hyp.14109>
- Webster, K., Leach, J. A., Houle, D., Hazlett, P. W., & Emilson, E. J. S. (2021). Acidification recovery in a changing climate: Observations from thirty-five years of stream chemistry monitoring in forested headwater catchments at the Turkey lakes watershed, Ontario. *Hydrological Processes*, 35(9), e14346. <https://doi.org/10.1002/hyp.14346>
- Webster, K. L., Leach, J. A., Hazlett, P. W., Buttle, J. M., Emilson, E. J. S., & Creed, I. F. (2022). Long-term stream chemistry response to harvesting in a northern hardwood forest watershed experiencing environmental change. *Forest Ecology and Management*, 519, 120345. <https://doi.org/10.1016/j.foreco.2022.120345>